Monthly Notices
of the
ROYAL ASTRONOMICAL SOCIETY

MNRAS **429,** 469–481 (2013) doi:10.1093/mnras/sts350

Pilot observations for MALT-45: a Galactic plane survey at 7 mm

C. H. Jordan,[1,2]★ A. J. Walsh,[1] V. Lowe,[2,3] N. Lo,[4] C. R. Purcell,[5] M. A. Voronkov[2] and S. N. Longmore[6]

[1]*Centre for Astronomy, School of Engineering and Physical Sciences, James Cook University, Townsville, QLD 4814, Australia*
[2]*Australia Telescope National Facility, CSIRO Astronomy and Space Science, PO Box 76, Epping, NSW 1710, Australia*
[3]*School of Physics, University of New South Wales, Sydney, NSW 2052, Australia*
[4]*Departamento de Astronomía, Universidad de Chile, Camino El Observatorio 1515, Las Condes, Santiago, Casilla 36-D, Chile*
[5]*School of Physics, University of Sydney, Sydney, NSW 2006, Australia*
[6]*ESO Headquarters, Karl-Schwarzschild-Str. 2, D-85748 Garching bei München, Germany*

Accepted 2012 November 2. Received 2012 October 26; in original form 2012 August 28

ABSTRACT

We introduce the Millimetre Astronomer's Legacy Team – 45 GHz (MALT-45) Galactic plane survey and describe pilot survey results with the Australia Telescope Compact Array (ATCA). The pilot survey was conducted to test the instrumentation and observational technique of MALT-45, before commencing the full survey. We mapped two half-square degree regions within the southern Galactic plane around the G333 giant molecular cloud, using fast mosaic mapping. Using the new Compact Array Broad-band Backend on the ATCA, we were able to observe two 2048 MHz spectral windows, centred on frequencies 43.2 and 48.2 GHz. Although only a coarse spectral resolution of around 7 km s^{-1} was available to us, we detect widespread, extended emission in the CS (1–0) ground state transition. We also detect eight Class I CH_3OH masers at 44 GHz and three SiO masers in vibrationally excited (1–0) transitions. We also detect the H53α radio recombination line, non-vibrationally excited SiO (1–0) and emission in the CH_3OH 1_1–0_0 A^+ line.

Key words: masers – surveys – stars: formation – ISM: molecules – Galaxy: structure – radio lines: ISM.

1 INTRODUCTION

High-mass stars have a pivotal influence on the structure of our Galaxy, particularly at the start and end of their lives. Young high-mass stars are responsible for the evolution of molecular clouds, for example, through their powerful, ionizing winds and the copious amounts of energy they inject into the interstellar medium (ISM) (Zinnecker & Yorke 2007). The energy a high-mass star exhibits over its lifetime can rival that of a supernova explosion. Finally, high-mass stars end their lives as supernovae, again dramatically altering the structures of the Galaxy, transforming the ISM and dispersing heavy elements.

High-mass star formation (HMSF) is a poorly understood process due to the rapid evolution of high-mass stars, rarity and high levels of dust extinction (Zinnecker & Yorke 2007). HMSF does not occur in isolation, thus making it difficult to disentangle mechanisms involved with HMSF from other sites of star formation in the vicinity. HMSF is known to occur within dense regions of giant molecular clouds (GMCs; e.g. Lo et al. 2011). In order to comprehend the earliest stages of HMSF, a catalogue of their regions must be identified and mapped through high-density tracers.

Previous surveys have been productive in identifying many sites of HMSF, but emphasize signposts that necessarily pick out only a subsection of the various stages. For example, methanol maser surveys (e.g. Walsh et al. 1998; Green et al. 2009) pick out hot cores and young ultracompact H II regions; infrared dark clouds (IRDCs; e.g. Rathborne, Jackson & Simon 2006) are only seen when they are close to us, and projected against a bright infrared background from the Galaxy and may not always identify sites of HMSF (Kauffmann & Pillai 2010); radio continuum sources are only found once a high-mass star has had time to reach the main sequence and push its ionizing wind through the surrounding material (e.g. Purcell & Hoare 2010).

Untargeted Galactic plane surveys not only give us an opportunity to address these concerns, but they also allow us to study aspects of HMSF on a Galaxy-wide scale, with higher resolution and sensitivity than is achievable in external galaxies. For example, we can study the structure of the Galaxy through CO surveys (e.g. Dame & Thaddeus 2008) and H I surveys (e.g. McClure-Griffiths et al. 2005). The nature of CO and H I mean that these tracers typically pick out low-density gas (10^{1-2} cm^{-3}) that is not directly related to HMSF. These tracers are also sensitive to interspiral arm gas, making it difficult to identify spiral structure in the Galaxy. Higher density gas tracers, such as NH_3 and HC_3N, observed as part of the H_2O southern Galactic plane survey (HOPS; Walsh et al. 2008, 2011), do

★ E-mail: christopher.jordan@jcu.edu.au

© 2012 The Authors
Published by Oxford University Press on behalf of the Royal Astronomical Society

Downloaded from http://mnras.oxfordjournals.org/ at Curtin University Library on December 5, 2013

trace gas directly associated with HMSF and may more clearly trace spiral structure. However, HOPS is a shallow survey, sensitive to typical HMSF regions within a few kpc. In order to study the spiral structure of the Galaxy, as well as the gas associated with HMSF, we have devised the MALT-45 survey. This paper introduces the MALT-45 survey design and outlines the autocorrelation results of pilot survey. MALT is the Millimetre Astronomer's Legacy Team – the result of a successful meeting of star formation astronomers to collaborate on major Southern hemisphere millimetre surveys. MALT currently consists of the MALT-90 (Foster et al. 2011) and MALT-45 surveys.

2 MALT-45 DESIGN

MALT-45 aims to provide a comprehensive survey of star formation tracers at 7 mm ($\sim$ 45 GHz) in the southern Galactic plane. MALT-45 is to be conducted on the Australia Telescope Compact Array (ATCA), exploiting the newly available technologies made by the Compact Array Broad-band Backend (CABB; Wilson et al. 2011). In particular, MALT-45 seeks to employ the CABB provided autocorrelations. Cross-correlation data are typically all that are used from an interferometer, as it provides the high-resolution imagery not available from a single dish. However, drawbacks in interferometery include gaps in the observed uv plane, meaning collected data are not completely represented. This is especially apparent for extended emission, such as CO, NH_3 and CS, as these uv-plane gaps will not reveal the full extent of extended emission. Autocorrelation data alleviate this by combining each antenna in an interferometer as if they were all single dishes, leaving no gaps in the uv plane. In this way, the CABB can be used to image extended emission with sensitivity similar to 6$\times$ Mopra (a single 22 m dish radiotelescope similar to a single ATCA antenna). Hence, MALT-45 achieves the advantages of using an interferometer to accurately position interstellar masers associated with HMSF, while simultaneously mapping the Galaxy for extended emission.

MALT-45 is an untargeted Galactic plane survey, covering a total of 30 square degrees, with a Galactic latitude width of $\pm 0.^{\circ}5$. The survey will focus on the dense gas tracer CS (1–0), and identify previously unknown sources of both Class I CH_3OH and SiO (1–0) masers, which occur towards sites of star formation and evolved stars, respectively. The survey region of MALT-45 will be a subsection of HOPS (which covers a range $l = 290^{\circ}$ through $l = 0^{\circ}$ to 30°, $b = \pm 0.^{\circ}5$). Other lines of possible interest are outlined in Table 1. The CABB allows a 64M–32k zoom mode configuration (see Section 2.3), which will be used to provide fine velocity resolution, while also covering a large velocity range.

2.1 Tracers

The ground state transition ($J = 1 - 0$) of CS is a high-density gas tracer (4.6×10^4 cm^{-3}; Evans 1999) that can be used in conjunction with HOPS NH_3 data to identify the regions of high density in our Galaxy. Apart from the slightly higher critical density of CS, compared to NH_3, CS is also known to freeze-out on to dust grains in the coldest and densest conditions (Tafalla et al. 2002), whereas NH_3 appears to be relatively robust against freeze-out (Bergin et al. 2002). CS can be carefully compared to NH_3 to identify these cold and dense regions (low CS/NH_3 ratio and NH_3 temperature) in our Galaxy, which identify the precursors to future star formation. We expect CS to be optically thick at some positions, but we are fortunate that $C^{34}S$ also occurs within the frequency band of MALT-45. A comparison of CS and $C^{34}S$ can give us a direct measure of the optical depth.

Methanol masers are separated into two classes: Class I and II. The better known and studied Class II masers are closely associated with HMSF (Walsh et al. 1998). The Class I masers are traditionally thought to be associated with outflows, offset from sites of star formation, although some evidence suggests there may be closer associations in some places (Voronkov et al. 2006). The strongest Class I methanol maser occurs at 44.069 GHz, in the 7 mm band, but it has not been searched using an untargeted survey. With the advent of 7 mm receivers on the ATCA, we will compare their occurrence to other masers, such as the Class II masers from the methanol multibeam survey (Green et al. 2009) and water masers from HOPS (Walsh et al. 2011) in an untargeted way.

SiO masers are typically associated with evolved AGB stars, where they occur at a few stellar radii in the extended atmosphere (Elitzur 1992). There are only three known sites of SiO masers towards star-forming regions (Orion, W51 and Sgr B2), despite extensive searches (Zapata et al. 2009). However, SiO masers in Orion provide some evidence of a high-mass accretion disc (Matthews et al. 2007). It is hoped that an untargeted survey for SiO masers will detect many previously unknown sources around late-type stars, and previously unknown masers associated with star formation. The ground state (thermal) SiO transition is commonly found in star formation regions and is a reliable tracer of outflows

Table 1. Spectral lines in the 42.2–49.2 GHz range. Radio recombination lines (RRL) are taken from Lilley & Palmer (1968). All other rest frequencies are taken from the Cologne Database for Molecular Spectroscopy (Müller et al. 2005).

Spectral line	Frequency (GHz)	Pilot survey detection	Maser or thermal?	Beam size (arcsec)
SiO (1–0) $v = 3$	42.519 34	N	Maser	66
SiO (1–0) $v = 2$	42.820 48	Y	Maser	66
H53α (RRL)	42.951 97	Y	Thermal	65
SiO (1–0) $v = 1$	43.122 03	Y	Maser	65
SiO (1–0) $v = 0$	43.423 76	Y	Thermal	65
CH_3OH 7(0,7)–6(1,6) A^+	44.069 41	Y	Maser (Class I)	64
H51α (RRL)	48.153 60	N	Thermal	58
$C^{34}S$ (1–0)	48.206 94	Y	Thermal	58
CH_3OH 1_1–0_0 A^+	48.372 46	Y	Thermal	58
CH_3OH 1_1–0_0 E	48.376 89	N	Thermal	58
OCS (4–3)	48.651 60	N	Thermal	58
CS (1–0)	48.990 95	Y	Thermal	57

Downloaded from http://mnras.oxfordjournals.org/ at Curtin University Library on December 5, 2013

(Martin-Pintado, Bachiller & Fuente 1992). MALT-45 will detect strong outflows from regions of HMSF, which will be the subject of future studies.

The CABB provides excellent sensitivity to continuum emission, even with very short integration times, given that two 2 GHz bands are observed simultaneously. MALT-45 is in the unique position of being a high-frequency untargeted survey, simultaneously collecting autocorrelated data. Since continuum emission is typically extended, we aim to use the autocorrelation data to image the continuum with arcminute resolution. Additionally, the 7 mm continuum cross-correlation data can be used to filter out extended emission to study ultracompact and hypercompact H II regions. With the CABB, we will also be able to measure the spectral index of continuum sources between 42.2 and 49.2 GHz. At MALT-45 frequencies, some continuum sources will be dominated by free–free emission and some by dust emission. The spectral index will allow us to discriminate between the two mechanisms of emission.

2.2 The G333 GMC

The MALT-45 pilot survey was conducted partially over the GMC associated with the H II region RCW 106. RCW106 has a centre located roughly at $l = 333^{\circ}, b = -0.^{\circ}5$. We are particularly interested in this GMC, commonly referred to as the G333 complex, located at a distance of 3.6 kpc (Lockman 1979). The G333 GMC has been thoroughly investigated for molecular spectral lines relevant to star formation (Bains et al. 2006; Wong et al. 2008; Lo et al. 2009), and has shown evidence of HMSF (Lo et al. 2011). See Bains et al. (2006), Wong et al. (2008) and Lo et al. (2009) for a detailed description of the G333 complex. G333 is an ideal location to test MALT-45 before commencing the full survey, as we can expect extended CS thermal emission and Class I CH_3OH masers to be detected (Slysh et al. 1994).

2.3 Pilot survey observations and data reduction

The first observations for MALT-45 were conducted on the ATCA over 36 h from 2010 March 18 to 20, using the H168 array configuration. Additional MALT-45 observations were conducted on 2010 June 7 and 8, using a 6C array configuration. These observations were necessary to test the feasibility of MALT-45, as conducting an untargeted survey at this frequency will be demanding on time, and may yield poor data if not allowed to observe optimally.

A mosaic of source pointings was constructed to observe over one square degree, with interleaved points spaced on a square grid of 42 arcsec, which is slightly larger than Nyquist sampled at the highest frequency (29 arcsec, assuming a beam of 57 arcsec). The mosaic contained roughly 12 000 points, and thus required short exposure times for each point to be completed within the allocated observation time; hence, only 6 s of observation was allowed for each pointing. Prior testing to the pilot survey revealed that the ATCA required nominally 1.5 s settling time between adjacent points, thus leaving at most 4.5 s per pointing. This pilot survey was also necessary to test the 6 s cycle time used instead of the ATCA default 10 s.

Due to software limitations, a single mosaic of 12 000 discrete pointings was not possible on the ATCA. Instead, it was split into two half-mosaics, observed one after the other. However, an unfortunate miscalculation on the position of each half-mosaic caused an approximate half-degree gap between each mosaic. Nevertheless, an entire square-degree was mapped as planned. The centres of each half-mosaic are approximately 333.°4 and 334.°1 in Galactic longitude.

At the time of observation, the CABB was unable to provide the 64M–32k zoom windows, providing only broad-band mode windows. The 64M–32k zoom windows, when completed and ready for use on the CABB, provide 16 simultaneous observing windows per 2048 MHz broad-band window, each with 2048 channels over 64 MHz, yielding a 32 kHz fine resolution. At the rest frequency of a Class I CH_3OH maser, each channel of a zoom window provides a resolution of approximately 220 m s^{-1}. Without the zoom modes, the ATCA provides two broad-band windows simultaneously, each with 2048 MHz of bandwidth, and 2048 channels. These windows were centred on frequencies of 43.2 and 48.2 GHz, and were placed to observe SiO (1–0) masers, Class I CH_3OH masers and CS (1–0) thermal emission. These spectral lines and hence the 2 GHz band placements have been selected as being easiest to detect without sacrificing too many other lines of interest, and therefore some lines are neglected (e.g. HCCCN at 45.490 31 GHz). As each channel corresponds to 1 MHz in the spectrum, the approximate resolution at these frequencies is a coarse 6.8 km s^{-1}. Future MALT-45 observations using the 64M–32k zoom windows on each of the 12 spectral lines listed in Table 1 will provide much higher channel resolution, resulting in more detailed velocity information.

In this paper, we focus on the autocorrelation data rather than interferometric data, as this is the most innovative data processing aspect of the MALT-45 pilot survey. As autocorrelation data reduction is not common on the ATCA, the procedure to make this imagery possible was developed by the authors. These steps include.

(i) Using MIRIAD tasks ATLOAD and UVAVER to first select autocorrelations from the raw data, and select specific channel ranges of the data applicable to emission.

(ii) Converting extracted ATCA CABB autocorrelations from the MIRIAD data set into an SDFITS format as if these data resulted from a single-dish with a 6 beam receiver, one beam per ATCA antenna.

(iii) Removing the baseline of the single-dish data using LIVEDATA. Each 'beam' presented corresponds to an individual antenna from the ATCA.

(iv) Producing data cubes with GRIDZILLA.

LIVEDATA parameters used include a referenced method with a mean estimator, a robust linear fit for baseline subtraction, and a Doppler frame of LSRK. The reference position used for baseline subtraction was G334.0−1.0, and was observed for 5 cycles (30 s) approximately every 34 min. GRIDZILLA parameters include a beam full-width at half-maximum (FWHM) of 1 arcmin, a kernel FWHM of 1.5 arcmin, a cutoff radius of 0.8 arcmin and a mean gridding statistic.

Once cubes are produced, they may be further manipulated in MIRIAD for analysis, such as producing peak-intensity maps. Cubes needed to be produced individually for each emission line, as the channel range that could be processed was small. At the time of observation, the CABB also had bad channel issues with the broad-band windows, specifically, in the channel range 250–500, and all multiples of 512.

It was found that data from antenna 6 of the ATCA (CA06) had increased noise levels by a factor of 3.5. The removal of CA06 data from the other antenna data improved the quality of images substantially. The source of the poorer performance of CA06 is suspected

Downloaded from http://mnras.oxfordjournals.org/ at Curtin University Library on December 5, 2013

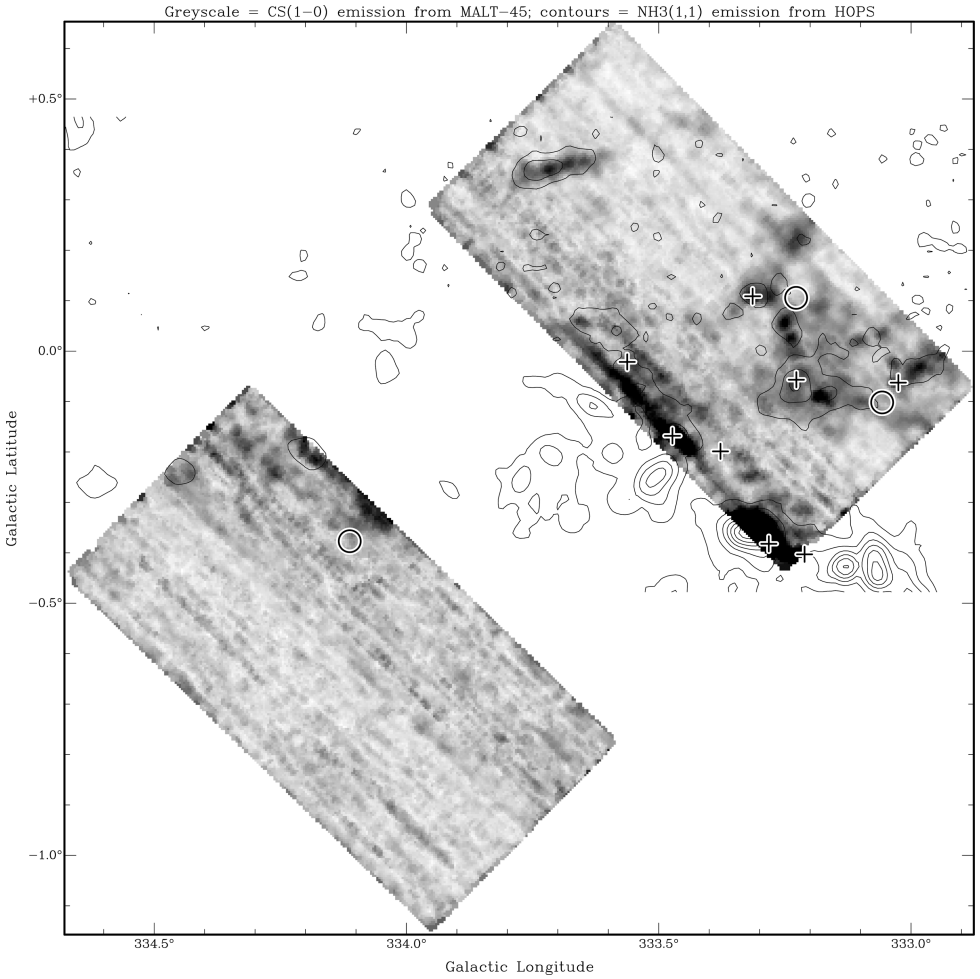

Figure 1. Autocorrelated CS peak-intensity map, overlaid with HOPS thermal NH_3 (1,1) contours. Contour levels are 10, 20, . . . ,90 per cent of 1.09 K in units of antenna temperature. Circles represent SiO $v = 2$ maser positions, while plus symbols (+) designate Class I CH_3OH maser positions.

to be due to the different dish surface, and its poor reception to 7 mm emission.

MIRIAD,[1] LIVEDATA and GRIDZILLA[2] are software packages managed and maintained by CSIRO Astronomy and Space Science.

3 RESULTS

Autocorrelated data cubes were produced for each of the lines listed in Table 1 from the ATCA broad-band data. We detected emission in CS (1–0) (Fig. 1), Class I CH_3OH masers at 44 GHz (Figs 2 and 3), vibrationally excited SiO masers (Figs 3 and 4), as well as occasional detections of H53α, SiO (1–0) $v = 0$ and CH_3OH 1_1–0_0 A^+. Radio recombination lines H53α and H51α were anticipated detections, as the brightest H69α detection in the Galactic plane found by HOPS is located at (333.609, −0.211). The survey region of this pilot survey did not cover the known regions of emission, but some H53α recombination line emission was found cospatial with the Class I CH_3OH maser located at (333.281, −0.382).

As only the broad-band modes were available at the time of observation, the results provide a coarse spectral resolution of about 6.8 km s^{-1}. Fortunately, some observing time was permitted on the Mopra radiotelescope to briefly follow up some of the detected Class I CH_3OH and SiO masers. Observations on Mopra were carried out using a standard position-switch mode, where each on-source position was observed for 5 min, resulting in a higher sensitivity than the ATCA observations. Maser emission characteristics are detailed in Table 2 and Figs 5 and 6.

The RMS noise level was calculated, based on the five antennas used in autocorrelated data, to be about 30 mJy $beam^{-1}$ (2 mK $beam^{-1}$ on the main beam brightness temperature scale) per single 6.8 km s^{-1} channel.

By comparing the positions of the same maser feature in G333.227−0.057, the estimated astrometric errors are derived from new ATCA data from Voronkov et al. (in preparation). We find an offset of 9 arcsec and so assign the estimated astrometric error of the pilot survey work to be 10 arcsec.

3.1 CS (1–0) at 48.990 GHz

The main isotopologue of CS was detected in extended emission across a large portion of the survey region (Fig. 1). Also shown in Fig. 1 is NH_3 (1,1) emission, as detected in HOPS (Purcell et al. 2012). The CS emission appears to closely follow the NH_3 emission, as might be expected from the two quiescent dense gas tracers (e.g. Purcell et al. 2009). The strongest CS emission occurs cospatial

[1] http://www.atnf.csiro.au/computing/software/miriad/
[2] http://www.atnf.csiro.au/computing/software/livedata/index.html

Downloaded from http://mnras.oxfordjournals.org/ at Curtin University Library on December 5, 2013

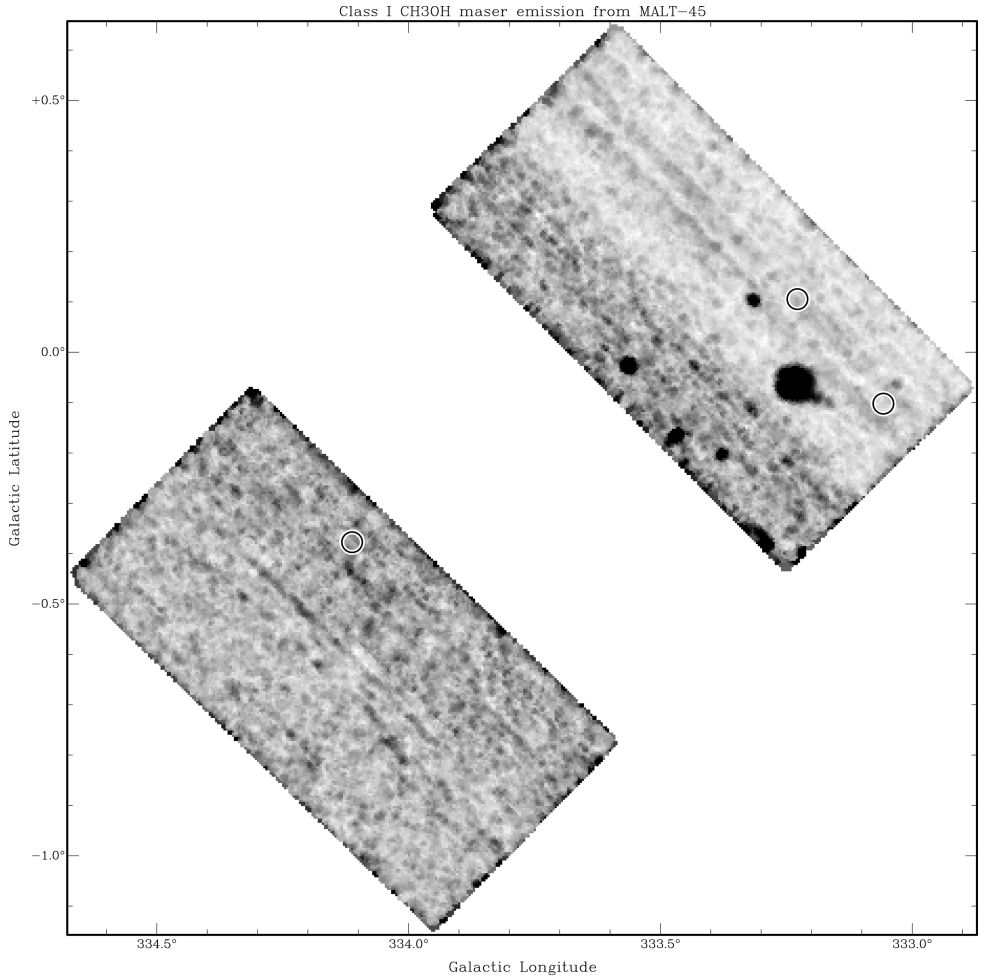

Figure 2. Autocorrelated Class I CH_3OH maser peak-intensity map. Circles represent SiO $v = 2$ maser positions.

with the G333 GMC, which is close to the edge of the surveyed area around (333.3, −0.4).

Extended CS emission is seen between Galactic longitudes of 329.9 and 333.3 and Galactic latitudes −0.2 and +0.3. Within this region NH_3 emission is detected, but covers a much smaller area than the CS emission, likely attributable to the relatively poor sensitivity of HOPS.

At (333.70, +0.35), we see a filamentary CS structure that is oriented close to the Galactic plane. This structure is also seen in NH_3 emission (Fig. 1), as well as an IRDC (Fig. 7). See Section 4.3 for more details.

3.2 Class I CH_3OH 7(0,7)–6(1,6) A $^+$ masers at 44.069 GHz

In the survey region, we found eight possible Class I CH_3OH masers, whose properties are listed in Table 2 and shown as grey-scale emission in Fig. 2, and positions are shown in Figs 1, 4, 7 and 8 as plus (+) symbols. Most of the masers (5 of 8) are cospatial with the G333 GMC and have line-of-sight velocities within 10 km s^{-1} of the GMC systemic velocity. They are thus likely to be associated with the star formation occurring in and around the GMC. The other three appear cospatial with extended CS emission. The CABB broad-band spectra for each maser are provided in Fig. 3. For each of these detections, we managed to acquire time on the Mopra radiotelescope to re-observe the CH_3OH spectra, as shown in Fig. 5. With the superior spectral resolution of Mopra, more convincing detections are made and finer velocity detail becomes apparent. Of all the CH_3OH detections, G333.227−0.057 has been previously reported as a detection at 44 GHz by Slysh et al. (1994) and G333.473−0.168 by Voronkov et al. (2012).

3.3 SiO (1–0) $v = 1, 2$ masers at 43.122 and 42.820 GHz

SiO emission in the vibrationally excited transitions, which are known to show maser activity, was tentatively detected towards three positions, shown as circles in Figs 1, 2, 7, and 8, and as grey-scale in Fig. 4. All three positions appear to exhibit emission in the $v = 2$ transition and two of the three in the $v = 1$ transition (the exception being G333.228+0.105). Spectra for the $v = 2$ transition are shown in Fig. 3. Again, emission is restricted to a small number of channels, using the CABB broad-band mode. Each of the three tentative masers were re-observed with Mopra and high-resolution spectra are provided for two in Fig. 6, where more detail of the spectra can be seen. The maser at G333.228+0.105 was not detected by Mopra, leaving its detection status by the CABB as tentative. Figs 7 and 8 show the locations of the SiO masers with respect to infrared emission from Galactic Legacy Infrared Mid-Plane Survey Extraordinaire (GLIMPSE). Each SiO maser is cospatial with a bright infrared star which is likely to be an evolved star in each case.

Downloaded from http://mnras.oxfordjournals.org/ at Curtin University Library on December 5, 2013

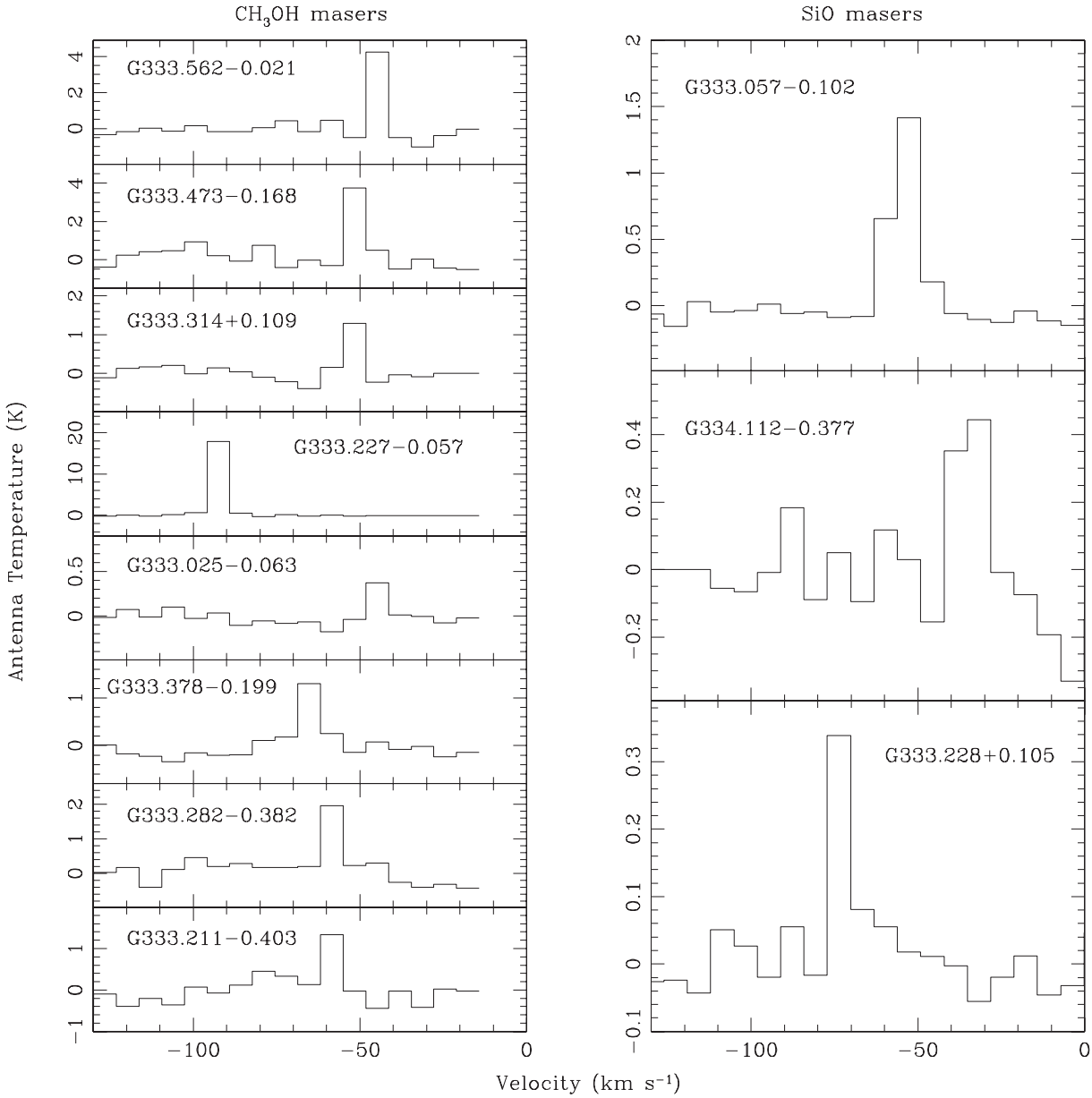

Figure 3. Autocorrelated spectra for each Class I CH_3OH (left) and SiO $v = 2$ maser (right) detected. The deviations in the baselines are a result of poor weather. The channel width is approximately 6.8 km s^{-1}.

3.4 Other detected lines

In addition to the main lines mentioned above, we made tentative detections in the SiO (1–0) $v = 0$ and CH_3OH 1_1–0_0 A^+ lines. The non-vibrationally excited state of SiO was detected towards G333.227−0.057, which is cospatial with a Class I CH_3OH maser. This SiO transition is usually associated with outflows from regions of star formation. Given the above, a star formation origin of this SiO emission is likely. The CH_3OH 1_1–0_0 A^+ and E lines are thermally emitting lines that are close in frequency (equivalent to 27.5 km s^{-1}). We detect thermal emission at G333.227−0.057 and G333.314+0.109 in the A^+ transition, but not the E transition. Kalenskii & Sobolev (1994) indicate that the E-CH_3OH transition may require higher densities to produce line strengths comparable to A^+-CH_3OH. The emission at G333.227−0.057 is cospatial with the thermal SiO source above and thermal methanol at G333.314+0.109 is cospatial with another Class I CH_3OH maser, leading to a likely star formation origin for both thermal CH_3OH sources.

4 DISCUSSION

4.1 Weather effects

As can be seen in Fig. 1, significant 'striping' artefacts exist in the data. The stripes coincide with the scanning direction of the observations. One contributing factor to the poor data is the fast-mosaic method; due to the fast transition times between pointings, some antennas were unable to keep up and did not contribute data. However, the main factor in poor data is the inclement weather experienced during observations. The most prominent stripes seen in Fig. 1 coincide with periods of light rain. Lagging antennas serve to decrease our sensitivity to emission, but the weather hampers our ability to determine real astrophysical emission from noise. This

Downloaded from http://mnras.oxfordjournals.org/ at Curtin University Library on December 5, 2013

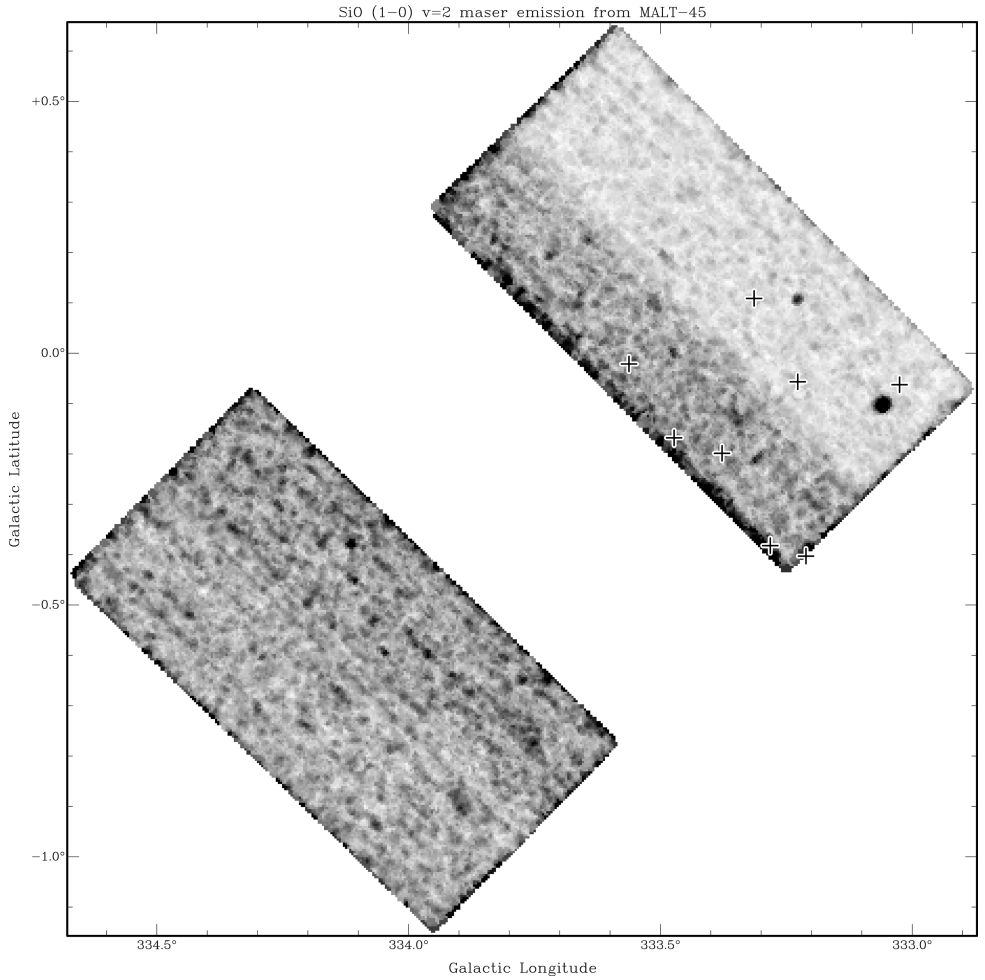

Figure 4. Autocorrelated SiO (1–0) $v = 2$ maser peak-intensity map. Plus symbols (+) represent Class I CH_3OH maser positions.

Table 2. Properties of detected MALT-45 maser emission as determined by Mopra.

Source name	RA (J2000) (h m s)	Dec. (J2000) (° ′ ″)	Peak antenna temperature (K)	Peak velocity (km s^{-1})	Velocity range Min (km s^{-1})	Max	Maser detected
G333.025−0.063	16 18 55.6	−50 24 03.6	0.34	−41	−42	−39	Class I CH_3OH
G333.057−0.102	16 19 15.0	−50 24 12.1	0.84	−48	−45	−50	SiO $v = 1, 2$
G333.211−0.403	16 21 15.6	−50 30 45.1	0.69	−52	−54	−51	Class I CH_3OH
G333.227−0.057	16 19 48.6	−50 15 17.2	18	−87	−86	−88	Class I CH_3OH
G333.282−0.382	16 21 29.0	−50 26 52.0	0.25	−52	−55	−50	Class I CH_3OH
G333.314+0.109	16 19 28.8	−50 04 45.0	0.70	−45	−45	−48	Class I CH_3OH
G333.378−0.199	16 21 05.8	−50 15 00.9	0.65	−61	−62	−56	Class I CH_3OH
G333.473−0.168	16 21 22.7	−50 09 42.6	1.1	−43	−42	−44	Class I CH_3OH
G333.562−0.021	16 21 08.1	−49 59 47.8	3.8	−40	−39	−41	Class I CH_3OH
G334.112−0.377	16 25 06.7	−49 51 28.5	0.14	−30	−29	−34	SiO $v = 1, 2$

weather introduced noise into both broad-band spectral windows, but has affected some frequencies more than others. See Fig. 3 for CH_3OH and SiO spectra. Examples of species with poor spectra include CH_3OH 1_1–0_0 A^+ (and its E species), H53α and H51α. The noise is apparent on all relevant frequencies of emission, but fortunately has permitted reasonable detections for the primary lines of interest (CS, Class I CH_3OH and SiO masers).

It must be mentioned that the problems experienced in the pilot will not plague the overall MALT-45 survey, as the pilot survey merely seeks to provide a proof of concept on the techniques used and reveals potential problems before committing to the full observation.

4.2 Telescope performance

Given the demands of our observational setup, we found some limitations to the ATCA that have affected the outcome of our pilot observations. Initially, we found software limitations that meant changes to the intended survey design. These included: mosaic scans in right ascension and declination coordinates only, rather

Downloaded from http://mnras.oxfordjournals.org/ at Curtin University Library on December 5, 2013

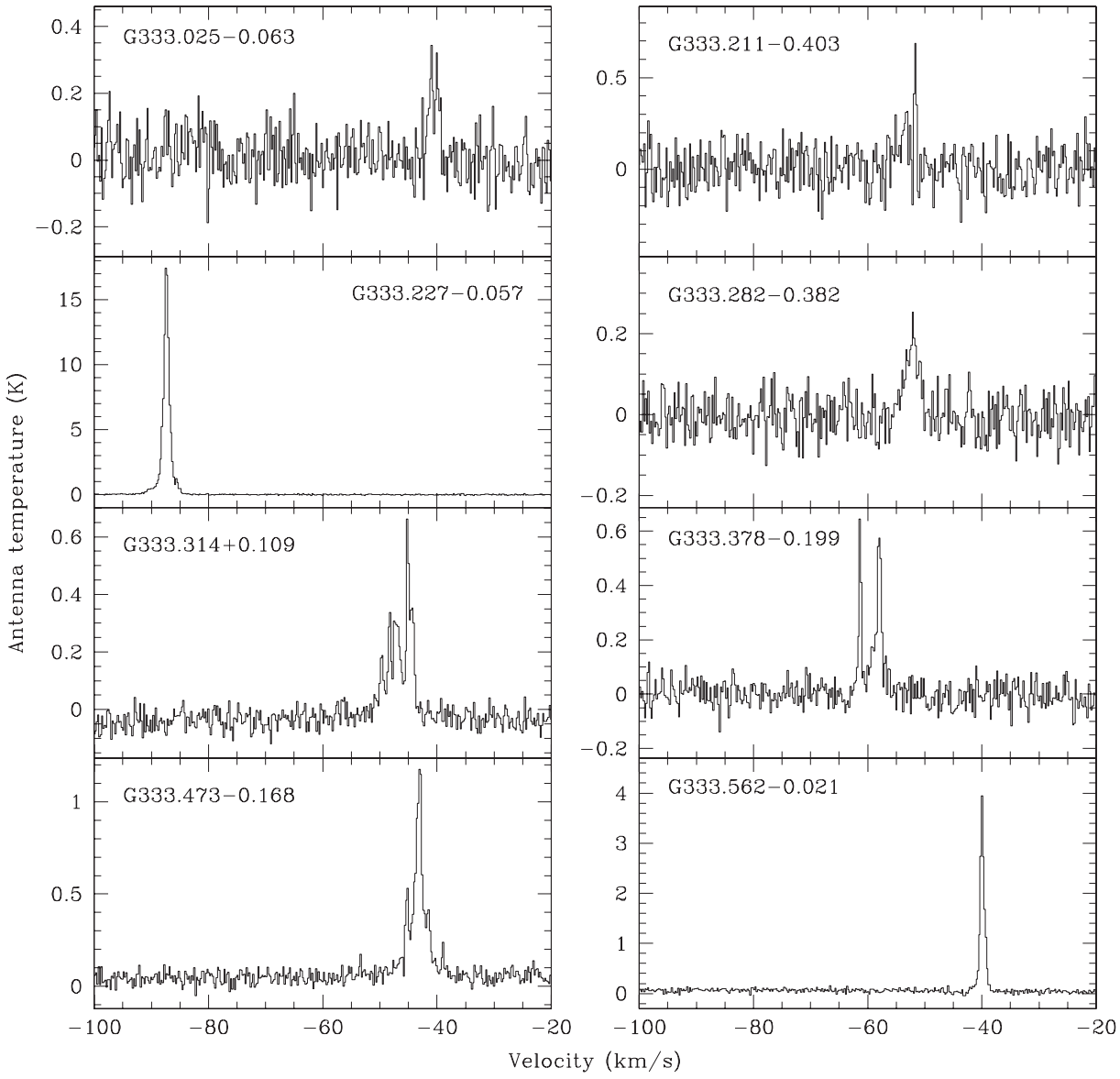

Figure 5. Follow-up Class I CH_3OH maser spectra from the Mopra radiotelescope.

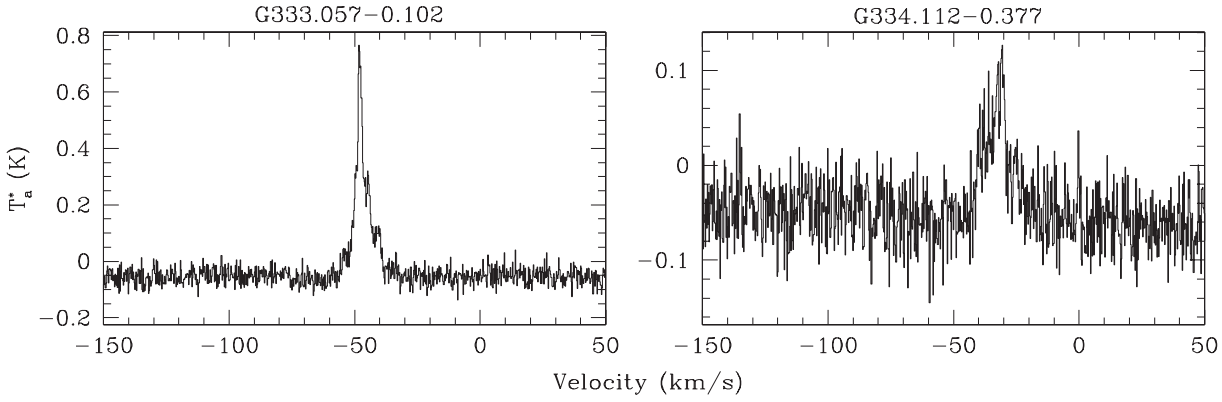

Figure 6. Follow-up SiO maser spectra from the Mopra radiotelescope.

Downloaded from http://mnras.oxfordjournals.org/ at Curtin University Library on December 5, 2013

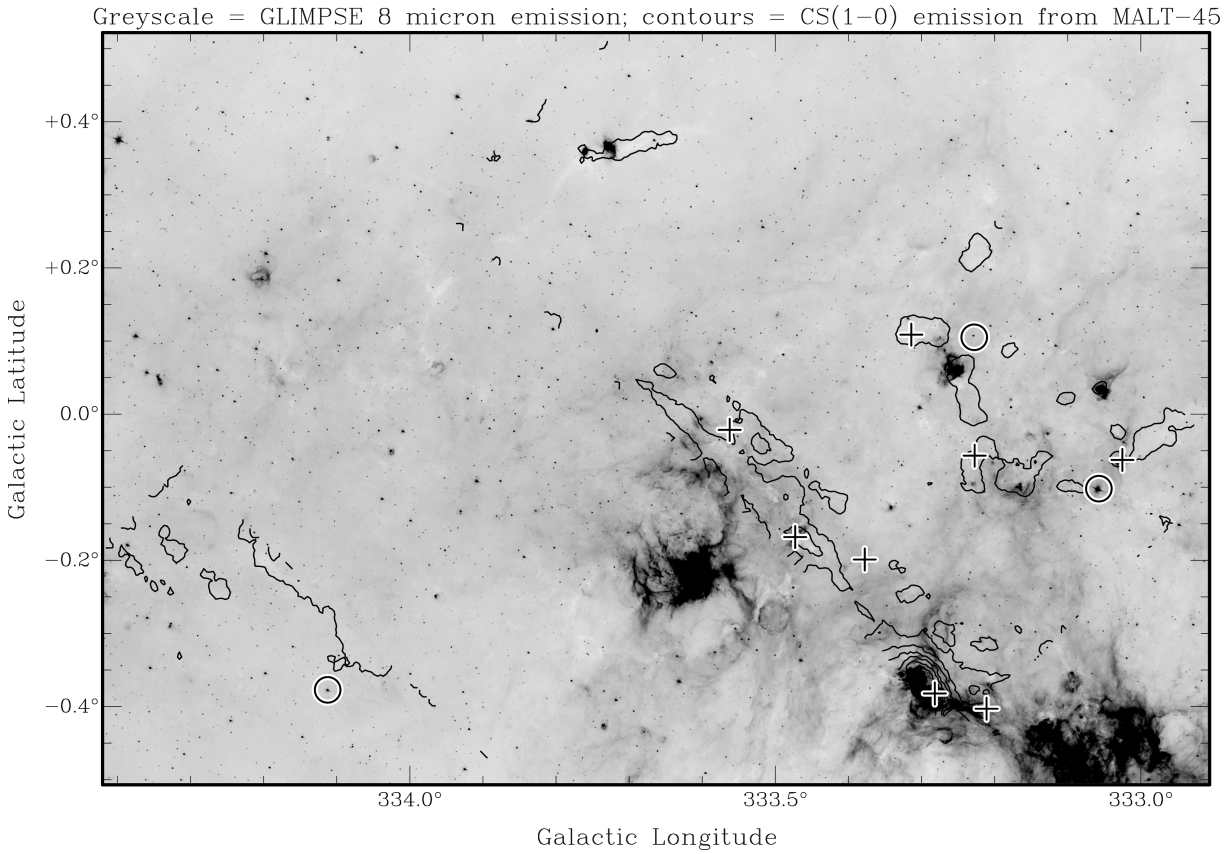

Figure 7. *Spitzer* GLIMPSE 8.0 μm grey-scale image with MALT-45 pilot survey CS (1–0) thermal emission in black contours, and positions of detected CH_3OH (plus) and SiO (circles) masers. Contour levels are 7, 17, . . . , 87 per cent of 0.72 K, in units of antenna temperature.

than Galactic coordinates; no more than 999 pointings per mosaic file; no more than 2000 individual commands in a schedule file. These limitations resulted in a survey region that is at an angle to the Galactic plane, as can be seen in Fig. 1, and a complicated mosaicking system.

During the observations, zoom modes with the CABB were not available, so we used the broad-band mode. This had the unfortunate effect of greatly limiting the amount of spectral detail seen, as described in Section 2.3. We also expect that the broad-band mode is less sensitive to narrow-line emission (e.g. masers) by a factor of up to 3. Also as mentioned previously, we found that some of the antennas had difficulty in keeping up with the demanding 6 s pointing regime. Indeed, we found that rms errors on the position of antenna 3 were typically 20 arcsec, which has reduced the sensitivity of the resulting data. We believe that these excessive pointing errors can be eliminated with on-the-fly (OTF) mapping, where the antennas are driven smoothly and subsequent testing of this method suggests OTF mapping will resolve this issue for the full survey.

4.3 Comparison with other observations

In this section, we compare selected sources within the MALT-45 pilot survey region to observations from previous surveys. In particular, we compare our results with the mid-infrared *Spitzer* GLIMPSE (Benjamin et al. 2003) for a visual correlation with infrared structures and objects. Mid-infrared extended emission is typically seen towards regions of active star formation, where the interstellar dust has been heated by newly formed stars. In addition to infrared emission, GLIMPSE also reveals prominent regions of infrared absorption, projected against the bright infrared background emission from the Galaxy. Such absorption features are referred to as IRDCs (Rathborne et al. 2006). These IRDCs are regions of high extinction where star formation may be about to take place in the near future, or has already taken place, but has not had sufficient time to break through the high extinction.

Infrared emission can also arise from a variety of other astrophysical objects. One such example is emission from evolved stars, that may also give rise to SiO masers, which appear as bright infrared stars in the GLIMPSE images (Robitaille et al. 2008). The evolved stars appear unresolved in the GLIMPSE images, which may occasionally be confused with confined sites of star formation. A useful, but not entirely robust, method to distinguish between evolved and young stars is that an infrared star is likely to be evolved if it is not associated with extended infrared emission or an IRDC and has a 4.5 μm magnitude brighter than 7.8 (Robitaille et al. 2008). Young stars are more likely to be fainter and associated with either extended emission or IRDCs.

A comparison of MALT-45 CS to HOPS NH_3 would be a valuable scientific addition to this paper, providing insight into star formation within these clouds. However, the data being presented are not of a sufficient quality to merit an accurate analysis. A variation in the CS/NH_3 ratio may be apparent in a region such as (333.24, +0.21), where there appears to be an overabundance of CS, relative to NH_3, as can be seen in Fig. 1. A thorough analysis will instead be performed with data from the full MALT-45 survey.

Downloaded from http://mnras.oxfordjournals.org/ at Curtin University Library on December 5, 2013

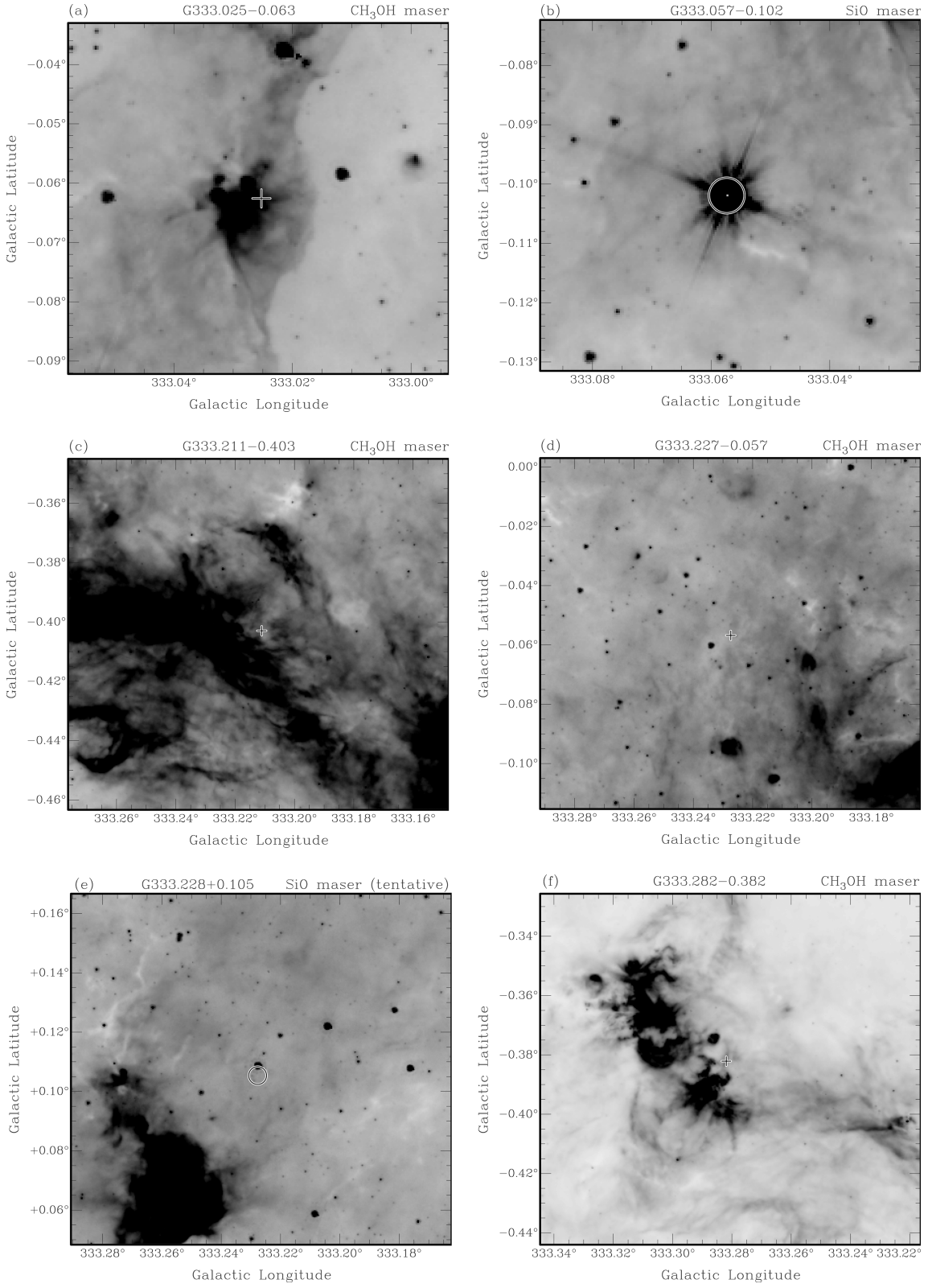

Figure 8. GLIMPSE 8 μm images of each region of maser detection. Plus (+) symbols designate positions of Class I CH_3OH masers, and circles represent SiO maser positions. (k) contours are CS (1–0) emission at 7, 9 and 11 per cent of 0.72 K, in units of antenna temperature.

Downloaded from http://mnras.oxfordjournals.org/ at Curtin University Library on December 5, 2013

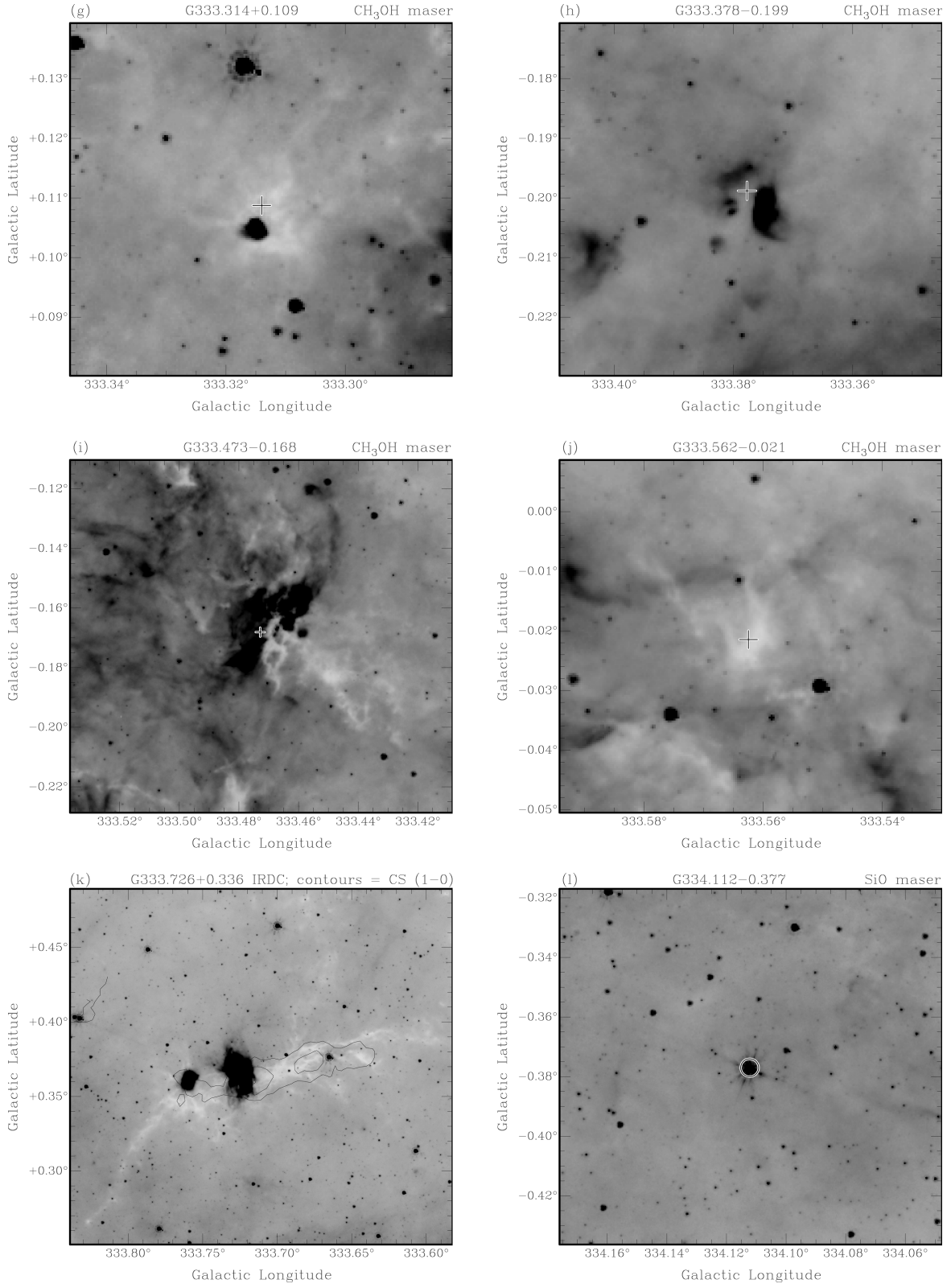

Figure 8 – *continued*

4.3.1 G333.227−0.057

GLIMPSE images in Figs 7 and 8 reveal that the region at G333.227−0.057 is on the edge of extended emission, but does not appear to be closely associated with a prominent infrared feature. We note there is an infrared source located approximately 15 arcsec to the lower-left of the maser position in Fig. 8(d), which could be the powering source for an outflow that creates the maser.

Downloaded from http://mnras.oxfordjournals.org/ at Curtin University Library on December 5, 2013

The Class I CH_3OH maser spectrum (Fig. 5) is dominated by a single peak at around -87 km s^{-1}. This region has been studied previously, and contains OH maser emission (Sevenster et al. 1997), Class II CH_3OH maser emission (Ellingsen et al. 1996) and water maser emission (Kaufmann et al. 1976; Breen et al. 2010). The spectra of all maser species are remarkably similar, with a peak close to -87 km s^{-1}, indicating a likely common origin for all masers. This velocity is significantly different from velocities of gas found associated with the G333 GMC, which are more typically around -45 km s^{-1}. Lockman (1979) calculate a distance of 3.6 kpc to G333. Based on a kinematic model of Galactic rotation, we estimate that the distance to G333.227−0.057 is 5.1 kpc, putting it at a significant distance behind G333.

The Class I CH_3OH maser associated with G333.227−0.057 was first detected by Slysh et al. (1994), with a peak flux density over 300 Jy. Using the high-velocity resolution Mopra observations (Fig. 5), we see that the spectrum shows weaker emission, with a peak flux density 250 Jy, assuming a Jy/K conversion factor of 14.1 (Urquhart et al. 2010). This difference may be partially due to intrinsic variability of the maser, but can likely be attributed to calibration uncertainties which are at the 20 per cent level.

We have detected unresolved SiO (1–0) $v = 0$ emission coincident with G333.227−0.057. This emission is seen in a single channel in the CABB data, but also as a well-defined single peak in the Mopra follow-up data. Based on the Mopra spectrum at this position, the SiO emission has an integrated intensity of 2.2 K km s^{-1}, a peak velocity of -88.6 km s^{-1} and line FWHM of 12.7 km s^{-1}. The velocity of the SiO emission is within 2 km s^{-1} of the peak of the Class I CH_3OH maser, suggesting that the two are associated. As previously discussed, this ground state thermal transition is known to trace outflows associated with star formation. Using the CABB data, we also tentatively detect thermal CH_3OH emission in the 1_0–0_0 A^+ transition. Since this transition was not covered by the Mopra follow-up observations, we cannot be certain that this is a real detection. If this is a real detection, then we can expect occasional detection of these thermal lines throughout the main MALT-45 survey, which will be useful to compare the thermal and masing properties of CH_3OH in such regions.

4.3.2 G333.726+0.366

The CS image shows a clear elongated structure at this position. Comparison with the GLIMPSE 8 μm image indicates that there is an IRDC, whose morphology closely follows that of the CS emission (Fig. 8). HOPS NH_3 emission also closely follows the CS emission and IRDC. The NH_3 emission is strongest at -34.9 km s^{-1} and the CS emission appears to peak close to this, although the velocity of the peak is not known accurately due to the broad-band channels of the CABB. The close velocity and shape suggest that both CS and NH_3 arise from the IRDC. The IRDC is cospatial with bright, extended emission at 8 μm which lies at the peak of both CS and NH_3 emission. The extent of the CS and NH_3 emission is almost 0.′2, which, assuming a distance of 3.6 kpc (Lockman 1979), is equivalent to a projected distance of 10 pc. The GLIMPSE image indicates that the IRDC may extend significantly beyond this.

4.3.3 G333.314+0.109

We detect both CS and a Class I CH_3OH maser emission at this position. The GLIMPSE image of this region shows a faint IRDC, with an extended and reddened emission feature within the IRDC. The peak of weak NH_3 emission appears at this position, as well as a water maser, detected in HOPS. All spectral features appear to peak around -45 km s^{-1}, which is similar to the velocity of the G333 GMC. It is likely that this cloud and the G333 GMC are located at a similar distance from us.

5 FUTURE WORK

The pilot survey has been successful in many ways, perhaps most notably with the successful autocorrelation data reduction for each of the spectral lines relevant to MALT-45. The pilot has detected extended CS emission, as well as eight Class I CH_3OH masers, two SiO masers in the $v = 1$ and 2 transitions, and another tentative detection in the $v = 2$ transition. We have also detected thermal emission in CS, SiO $v = 0$ and CH_3OH 1_0–0_0 A^+ detections, with CS emission being extended across a large fraction of the surveyed area. However, we anticipate great improvements for the main survey, based on the results of this work, and the expected completion of the CABB upgrade on the ATCA.

With CABB 64M–32k zoom modes available, we expect to achieve spectral channel resolution of ∼0.2 km s^{-1}, which will not only allow us to identify more spectral features, but will also effectively increase our sensitivity to narrow-lined emission, such as from masers. For a maser of line 1 km s^{-1} FWHM, we expect to gain a factor of ∼2.5 in sensitivity.

We expect to employ an OTF mapping technique, which will eliminate problems with the antenna drive systems not being able to keep up with the rigorous 6 s pointing we have used in this work. Early tests using OTF have indeed proven this to be the case. Overall, this could increase sensitivity by a factor of about 2, as some mapped regions had only three antennas sufficiently close to the desired pointing position to have usable data.

Early problems with the CABB blocks that cause noisy channels to be flagged out (as mentioned in Section 4.2) should be greatly reduced, as the cause of such problems become identified. We are currently aware that the problems with some blocks have already been addressed.

The ATCA scheduler now allows us to write schedule files in Galactic coordinates, as well as allowing many more pointings per mosaic and commands per schedule file. This will allow for a much smoother running schedule, as well as a smoother final mapped region, without jagged edges that would be a result of RA/Dec. scans.

We will employ a method of scanning in two orthogonal directions (Galactic longitude and latitude). We expect that this will greatly reduce stripe features that are evident in the current data. Such stripes are mainly caused by varying weather conditions, but can also be affected by the changing elevation of the observations. Our experience in the pilot work is that observations should not be undertaken under heavy cloud, light rain or worse weather conditions. Scanning in two directions has proven very successful for OTF mapping with the Mopra radiotelescope, such as those used in HOPS. Scanning in two directions will also increase the sensitivity. Furthermore, the combination of both OTF mapping and orthogonal scans will produce data that are effectively Nyquist sampled with closest spacing between adjacent observations of 30 arcsec. Overall, we expect the sensitivity to masers in the full MALT-45 survey to be around 0.1 Jy. The differences between both surveys are highlighted in Table 3.

Downloaded from http://mnras.oxfordjournals.org/ at Curtin University Library on December 5, 2013

Table 3. MALT-45 parameters from the pilot survey and full survey.

MALT-45	Correlator configuration	Channel resolution (km s^{-1})	Cycle time (s)	Targeted spectral lines	OTF mapping	Orthogonal scans/ Nyquist sampling
Pilot survey	2 × 2048 MHz broad-band windows	∼7	6	12	No	No
Full survey	32 × 64 MHz zoom windows	∼0.2	6	12	Yes	Yes

ACKNOWLEDGMENTS

We acknowledge and thank the referee, J. Martin-Pintado, for his comments that have improved the quality of this paper. We thank CSIRO Astronomy and Space Science for allowing the use of the ATCA in this project, and for the development of CABB. We thank the staff at Narrabri for their assistance and testing of the small mosaic transition timings on the ATCA before the pilot survey observations. NL acknowledges partial support from the ALMA-CONICYT Fund for the Development of Chilean Astronomy Project 31090013, Center of Excellence in Astrophysics and Associated Technologies (PFB 06) and Centro de Astrofísica FONDAP 15010003. The Australia Telescope Compact Array and the Mopra radio telescope are part of the Australia Telescope National Facility which is funded by the Commonwealth of Australia for operation as a National Facility managed by CSIRO.

REFERENCES

Bains I. et al., 2006, MNRAS, 367, 1609
Benjamin R. A. et al., 2003, PASP, 115, 953
Bergin E. A., Alves J., Huard T., Lada C. J., 2002, ApJ, 570, L101
Breen S. L., Caswell J. L., Ellingsen S. P., Phillips C. J., 2010, MNRAS, 406, 1487
Dame T. M., Thaddeus P., 2008, ApJ, 683, L143
Elitzur M., 1992, ARA&A, 30, 75
Ellingsen S. P., von Bibra M. L., McCulloch P. M., Norris R. P., Deshpande A. A., Phillips C. J., 1996, MNRAS, 280, 378
Evans N. J., 1999, ARA&A, 37, 311
Foster J. B. et al., 2011, ApJS, 197, 25
Green J. A. et al., 2009, MNRAS, 392, 783
Kalenskii S. V., Sobolev A. M., 1994, Astron. Lett., 20, 91
Kauffmann J., Pillai T., 2010, ApJ, 723, L7
Kaufmann P. et al., 1976, Nat, 260, 306
Lilley A. E., Palmer P., 1968, ApJS, 16, 143
Lo N. et al., 2009, MNRAS, 395, 1021
Lo N., Redman M. P., Jones P. A., Cunningham M. R., Chhetri R., Bains I., Burton M. G., 2011, MNRAS, 415, 525
Lockman F. J., 1979, ApJ, 232, 761
Martin-Pintado J., Bachiller R., Fuente A., 1992, A&A, 254, 315
Matthews L. D., Goddi C., Greenhill L. J., Chandler C. J., Reid M. J., Humphreys E. M. L., 2007, in Chapman J. M., Baan W. A., eds, IAU Symp. 242, Astrophysical Masers and their Environments. Cambridge Univ. Press, Cambridge, p. 130
McClure-Griffiths N. M., Dickey J. M., Gaensler B. M., Green A. J., Haverkorn M., Strasser S., 2005, ApJS, 158, 178
Müller H. S. P., Schlöder F., Stutzki J., Winnewisser G., 2005, J. Mol. Struct., 742, 215
Purcell C. R., Hoare M. G., 2010, Highlights Astron., 15, 781
Purcell C. R. et al., 2009, A&A, 504, 139
Purcell C. R. et al., 2012, MNRAS, 426, 1972
Rathborne J. M., Jackson J. M., Simon R., 2006, ApJ, 641, 389
Robitaille T. P. et al., 2008, AJ, 136, 2413
Sevenster M. N., Chapman J. M., Habing H. J., Killeen N. E. B., Lindqvist M., 1997, A&AS, 124, 509
Slysh V. I., Kalenskii S. V., Valtts I. E., Otrupcek R., 1994, MNRAS, 268, 464
Tafalla M., Myers P. C., Caselli P., Walmsley C. M., Comito C., 2002, ApJ, 569, 815
Urquhart J. S. et al., 2010, PASA, 27, 321
Voronkov M. A., Brooks K. J., Sobolev A. M., Ellingsen S. P., Ostrovskii A. B., Caswell J. L., 2006, MNRAS, 373, 411
Voronkov M. A., Caswell J. L., Ellingsen S. P., Breen S. L., Britton T. R., Green J. A., Sobolev A. M., Walsh A. J., 2012, in Booth R. S., Humphreys E. M. L., Vlemmings W. H. T., eds, IAU Symp. 287, Cosmic Masers – From OH to H_0. Cambridge Univ. Press, Cambridge, p. 433
Walsh A. J., Burton M. G., Hyland A. R., Robinson G., 1998, MNRAS, 301, 640
Walsh A. J., Lo N., Burton M. G., White G. L., Purcell C. R., Longmore S. N., Phillips C. J., Brooks K. J., 2008, PASA, 25, 105
Walsh A. J. et al., 2011, MNRAS, 416, 1764
Wilson W. E. et al., 2011, MNRAS, 416, 832
Wong T. et al., 2008, MNRAS, 386, 1069
Zapata L. A., Menten K., Reid M., Beuther H., 2009, ApJ, 691, 332
Zinnecker H., Yorke H. W., 2007, ARA&A, 45, 481

This paper has been typeset from a TEX/LATEX file prepared by the author.

Downloaded from http://mnras.oxfordjournals.org/ at Curtin University Library on December 5, 2013